Sustainable Energy & Fuels

Rapid Laser Synthesis of Medium-Entropy Alloy Nanostructures for Neutral Seawater Electrolysis

Journal:	*Sustainable Energy & Fuels*
Manuscript ID	SE-ART-11-2024-001572.R1
Article Type:	Paper
Date Submitted by the Author:	06-Jan-2025
Complete List of Authors:	Tan, Richard; University of Missouri Columbia, Department of Mechanical and Aerospace Engineering Xie, Yunchao; Miami University, Department of Mechanical and Manufacturing Engineering Chen, Zhenru; University of Missouri Columbia, Department of Mechanical and Aerospace Engineering Lin, Jian; University of Missouri Columbia, Department of Mechanical and Aerospace Engineering

Rapid Laser Synthesis of Medium-Entropy Alloy Nanostructures for Neutral Seawater Electrolysis

Richard Tan[1], Yunchao Xie[2*], Zhenru Chen[1], and Jian Lin[1*]

[1]Department of Mechanical and Aerospace Engineering
University of Missouri, Columbia, MO 65201, United States
[2]Department of Mechanical and Manufacturing Engineering
Miami University, Oxford, OH 45056, United States
[*]Email: xiey54@miamioh.edu; LinJian@missouri.edu.

Abstract

Seawater electrolysis powered by surplus renewable energy has garnered significant attention as part of global efforts towards carbon neutrality and climate change mitigation. Current mainstream seawater electrolysis primarily relies on alkaline or acidic electrolytes, which presents ongoing challenges due to their high costs and substantial maintenance requirements. As a result, neutral seawater electrolysis is emerging as a more attractive alternative, given its abundance. It remains a challenge due to its high salt content. In this work, we report the direct laser-induced synthesis of a medium-entropy alloy nanoparticles (MEA NPs), FeNiCoRu, as a bifunctional electrocatalyst for neutral seawater electrolysis. The unique features of direct laser induction including ultrahigh temperature, rapid heating/cooling rates enable the formation of homogeneous FeNiCoRu MEA NPs without phase separation. The FeNiCoRu MEA NPs exhibit the highest catalytic activity for hydrogen evolution reaction (HER) and oxygen evolution reaction (OER) among their single, binary, and ternary counterparts. Specifically, overpotentials of -0.368 V and -0.448 V are required for HER, while overpotentials of 0.559 V and 0.652 V are needed for OER to deliver current densities of 10 mA/cm^2 and 50 mA/cm^2, respectively. When assembled into an electrolyzer, FeNiCoRu||FeNiCoRu demonstrated an acceptable stability with a voltage increase of 0.161 V after 270 hours of continuous operation. The enhanced performance is attributed to the synergistic effects of the multi-elemental composition, particularly the role of Ru in reducing reaction barriers. Our findings demonstrate that direct laser-induced synthesis is a viable approach to develop advanced multi-component electrocatalysts, presenting a feasible solution for efficient neutral seawater electrolysis and the large-scale generation of green hydrogen.

Keywords: neutral seawater electrolysis, medium-entropy alloy, direct laser induction

1. Introduction

Green hydrogen plays a crucial role in decarbonization by providing a clean, renewable energy source that can replace fossil fuels in various industries, such as transportation and heavy manufacturing industry.[1] Currently, alkaline and acidic electrolysis using freshwater, powered by surplus offshore renewable energy sources, has the potential to revolutionize the energy landscape.[2-3] However, the widespread adoption of these technologies is hindered by considerable challenges, particularly the limited and uneven global distribution of freshwater resources. Seawater, which comprises 96.5% of Earth's water resources, represents a more abundant and potentially sustainable alternative. As such, seawater electrolysis has emerged as a transformative technology, achieving substantial advancements in recent years.[4-10] For example, Xie and colleagues developed a direct seawater electrolysis system that incorporates a self-breathable waterproof membrane and an self-dampening electrolyte into the electrolyzer.[4] This innovative approach effectively addresses side-reactions and corrosion issues, allowing the demonstrated system to operate stably for over 3000 hours at a current density of 250 mA/cm^2. In another example, Guo et al. introduced a Lewis acid layer of chromium oxide over transitional metal oxides to modulate the local reaction environment.[5] This modification facilitates hydrogen evolution reaction (HER) kinetics while preventing undesirable precipitation. Nevertheless, the high costs associated with acidic or alkaline chemicals and electrolyzer device present ongoing challenges, making natural seawater electrolysis more attractive in consideration of the high salt contents.[11-13] Therefore, the development of robust electrocatalysts that exhibit high activity and maintain long-term stability in neutral seawater is crucial to achieving industrial viability.

Currently, mainstream electrocatalysts mainly focus on noble metal electrocatalysts such as Pt/C for HER and IrO_2/RuO_2 for oxygen evolution reaction (OER).[14] However, However, the high

cost, scarcity, limited utilization efficiency, and poor durability of noble metals (Pt, Ru, and Ir) significantly hinder their large-scale commercialization.[15] At the same time, the catalytic activity and selectivity of transition metals (Fe, Ni, and Co) remain insufficient to fully replace noble metals.[16] Alloying an active metal with other inexpensive, stable, and catalytically active metals represents one of the most effective strategies to enhance catalytic activity, increase noble metal utilization efficiency, and reduce costs. The rising demand for novel alloys with superior properties necessitates a paradigm shift in alloy design, moving beyond conventional approaches toward the development of unconventional alloys.

Recently, medium/high entropy alloys, containing three or more principal metals in a single-phase crystal structure, have demonstrated remarkable performance in various catalytic applications.[17-20] They possess numerous unique features like abundant and active metal-metal interfaces, continuously changed adsorption energy, inherent thermal and chemical stability, and outstanding corrosion resistance, thus holding a great promise for the next-generation electrocatalysts.[18, 21] For example, Wang and coworkers prepared TiNbTaCrMo high entropy alloy (HEA) nanoparticles (NPs) using confinement assisted arc and plasma shock method and explored it for HER in natural seawater (pH = 8.3).[22] TiNbTaCrMo HEA NPs required an overpotential of 0.97 V to deliver a current density of 50 mA/cm^2. Kang et al. developed in-situ electrodeposited spinel-structured high entropy oxides/NiFeCuMoMn HEA multiphase electrocatalysts and showed an overpotential of 0.371 V at 10 mA/cm^2.[23] However, the HER performance of these materials significantly lags behind those achieved in acidic or alkaline electrolytes, hindering the practical applications. Additionally, the synthesis procedures are often complex, requiring specialized equipment. Therefore, developing a simple and efficient method for fabricating medium/high-entropy alloys for effective neutral seawater electrolysis is highly desired.

Herein, we present direct laser-induced synthesis of a medium entropy alloy (MEA), FeNiCoRu in the form of nanoparticles (NPs) as a bifunctional catalyst for neutral seawater electrolysis. The direct CO_2 laser induction technique offers exceptionally ultrahigh temperatures (>3200 K) along with ultrafast heating and cooling rates (up to 10^5 K/s). These conditions enable the formation of FeNiCoRu NPs with a homogeneous face-centered cubic (FCC) crystal structure. Material characterizations show no observable phase separation, which is often a limitation in the synthesis of multi-component alloys. FeNiCoRu NPs show superior electrocatalytic performance for HER and OER in neutral seawater compared to their single-element, binary, and ternary alloy counterparts. Specifically, they require overpotentials of only -0.368 V and -0.392 V to achieve current densities of 10 mA/cm^2 and 50 mA/cm^2, respectively, for HER. For OER, they necessitate an overpotential of 0.613 V to reach a current density of 10 mA/cm^2. When assembled into an electrolyzer, FeNiCoRu||FeNiCoRu demonstrated an acceptable stability with a voltage increase of 0.161 V after 270 hours of continuous operation. The enhanced electrocatalytic performance of FeNiCoRu NPs can be attributed to the synergistic effects arising from multi-elemental compositions, particularly the incorporation of Ru playing a critical role in lowering reaction barriers and improving catalytic efficiency. The combination of multiple transition metals not only optimizes active site properties but also contributes to improved chemical stability for effectively mitigating degradation in neutral seawater conditions. This work highlights the promise of FeNiCoRu NPs in bridging the gap between conventional electrocatalysts and practical, large-scale neutral seawater electrolysis, offering a pathway towards efficient green hydrogen generation. It also underscores the potential of direct laser-induced synthesis as a viable approach for fabricating advanced multi-component catalysts for various applications.

2. Results and Discussion

As shown in **Figure 1a**, FeNiCoRu NPs on a carbon paper were synthesized using a direct CO_2 laser induction method that we previously demonstrated.[20] The synthesis involved the following steps: First, a specific volume of metal-citrate complexes, including metal chlorides ($FeCl_3$, $NiCl_2$, $CoCl_2$, and $RuCl_3$) along with sodium citrate as a chelating agent, was drop-cast onto a precleaned carbon paper (**Table S1**). After allowing the carbon paper to dry, a commercial CO_2 laser was employed to irradiate both sides of the carbon paper under predetermined parameters, facilitating the reduction of metal-citrate complexes and the formation of single-phase solid solution of FeNiCoRu NPs. This laser-induced synthesis not only ensures efficient energy input but also enables rapid conversion under ambient conditions. The method achieves an ultrahigh temperature of > 3200 K and an ultrafast heating and quenching rates of 10^5 K/s.[20] The induced high temperature enhances atomic mobility, allowing different metal atoms to be homogeneously distributed within the particales.[20, 24] The ultrafast heating rate ensures that the metal precursors rapidly reach the decomposition temperature, while the rapid quenching rate helps to stabilize the desired structure without phase separation.[20, 24] These created far-from-equilibrium conditions are unique in formation of metastable phases and homogeneous solid solutions in a few seconds, which are hard to be synthesized by traditional approaches. In addition, far-from-equilibrium conditions can cause abundant defects within the nanoparticles.[25-26] After laser synthesis, the treated carbon paper was thoroughly washed with deionized water to remove any unreacted salts or by-products and was then dried for subsequent characterization and electrochemical testing. This approach effectively combines simplicity and scalability, making it suitable for synthesizing metal alloy NPs with potential applications in catalysis and energy storage.

The scanning electron microscope (SEM) image in **Figure 1b** reveals that FeNiCoRu NPs possess a porous, three-dimensional interconnected structure and microscale roughness. This unique morphology is highly advantageous, providing a high surface area that enhances the accessibility of active sites and increases the number of available reaction points—critical factors for catalytic applications.[27] The interconnected porous structure facilitates diffusion of reactants and promotes contact of the reactants with the catalyst. More importantly, the microscale roughness of the FeNiCoRu NPs plays a crucial role in electrochemical performance.[28-29] It allows for effective electrolyte infiltration, enhancing wettability and ensuring the uniform distribution of the electrolyte throughout the porous structure, which significantly boosts the catalytic reaction rate. Additionally, the rough surface promotes the release of gas bubbles (hydrogen and oxygen). By effectively dislodging gas bubbles from the catalyst surface, it prevents the blockage of active sites and reduces the risk of detachment of FeNiCoRu NPs, which can otherwise reduce electrocatalytic activity and long-term stability.

The high-resolution transmission electron microscope (HRTEM) image shows ordered lattice fringes with an interplanar spacing of 0.22 nm (**Figure 1c**), corresponding to the (111) plane of the face-centered cubic (FCC) structure of FeNiCoRu NPs, further confirming the crystalline nature of the synthesized NPs. Additionally, the corresponding elemental mapping image reveals a homogeneous distribution of the four metal elements—Fe, Ni, Co, and Ru—without any evident phase separation or segregation (**Figure 1d**). This uniform distribution is crucial for consistent catalytic performance. It suggests that the direct CO_2 laser induction method effectively produced a stable, single-phase solid solution. Such a homogeneous distribution of metal elements, coupled with the porous structure,[11] makes FeNiCoRu NPs a promising candidate for an electrocatalyst.

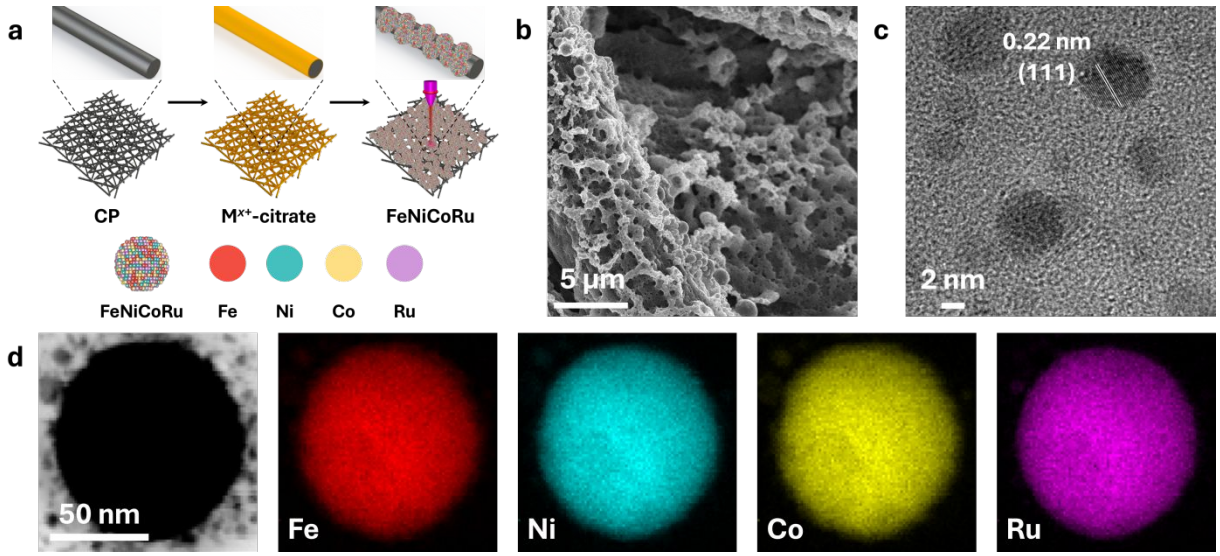

Figure 1. (**a**) Schematics showing synthesis steps of FeNiCoRu NPs using a CO_2 laser. (**b**) SEM, (**c**) TEM, (**d**) high-angle annular dark-field STEM (HAADF-STEM) and energy dispersive X-ray (STEM-EDX) elemental mapping images of FeNiCoRu NPs.

X-ray diffraction (XRD) patterns were conducted to investigate the crystallinity and phase composition of FeNiCoRu NPs. As shown in **Figure 2a**, FeCoCrRu NPs exhibit four diffraction peaks, with the first two at 42.8 and 49.7 corresponding to the (111) and (200) planes of an FCC structure (JCPDS 04-0850), and the other two at 44.4 and 53.7 are attributed to graphic carbon paper.[30-31] Close observation shows that the introduction of Co and Ru into FeNi to form FeNiCoRu NPs causes a significant blue shift of the (111) plane, indicating presence of abundant lattice distortion in FeNiCoRu crystal structure.[20] This distortion is primarily due to lattice mismatch and changes in bond distances resulting from the partial substitution of Ni sites with Fe, Co, and Ru atoms.[20] Moreover, the absence of the peaks related to separated metals or their oxides in all three samples strongly confirms the direct CO_2 laser induction is a powerful technique for synthesizing single-phase solid solution NPs under the ambient conditions.

X-ray photoelectron spectroscopy (XPS) was used to determine the chemical composition and valence states of FeNiCoRu NPs. The survey spectrum in **Figure 2b** validates the existence of Fe, Ni, Co, Ru, C, and O elements. Regarding the high-resolution Fe 2p spectrum (**Figure 2c**), the peaks at 709.6 eV and 718.3 eV correspond to metallic Fe^0 $2p_{3/2}$ and Fe^0 $2p_{1/2}$, respectively.[20, 31] Four additional peaks at 711.0 eV, 722.0 eV, 712.9 eV, and 723.9 eV, along with two satellite peaks at 715.3 eV and 725.7 eV, indicate the presence of Fe^{2+} and Fe^{3+} oxidation states. For high-resolution Ni 2p spectrum (**Figure 2d**), the peaks at 853.3 eV and 870.7 eV correspond to metallic Ni^0 $2p_{3/2}$ and Ni^0 $2p_{1/2}$, respectively. Peaks at 855.6 eV and 872.4 eV, along with satellite peaks at 861.8 eV and 879.9 eV, can be indexed to Ni^{2+} $2p_{3/2}$ and Ni^{2+} $2p_{1/2}$, respectively.[20, 32] The high-resolution Co 2p spectrum in **Figure 2e** was split into two components: metallic Co^0 (781.0 eV and 796.8 eV) and oxidized Co^{2+} (786.5 eV, and 803.2 eV).[20, 32] The high-resolution Ru 3p spectrum shows the presence of metallic Ru and ruthenium oxides (**Figure 2f**). The peaks at 461.9 and 483.8.4 eV correspond to Ru^0 $3d_{5/2}$ and Ru^0 $3d_{3/2}$, respectively, and the other two peaks at 464.7 eV and 485.7 eV are attributed to $Ru^{\delta+}$ $3d_{5/2}$ and $Ru^{\delta+}$ $3d_{3/2}$, respectively.[20, 33] Notably, Ru predominantly exists in the metallic state compared to Fe, Ni, and Co, which enhances the number of electroactive Ru sites, potentially improving catalytic activity.[34] In addition, the high-resolution O 1s spectrum (**Figure S1**) was deconvoluted into three subpeaks, correlating to lattice oxygen in amorphous metal oxides (530.1 eV), vacancy oxygen (530.8 eV), and adsorbed oxygen (532.0 eV), respectively.[20, 31] These results reveal that FeNiCoRu NPs possess both oxidized and metallic states.

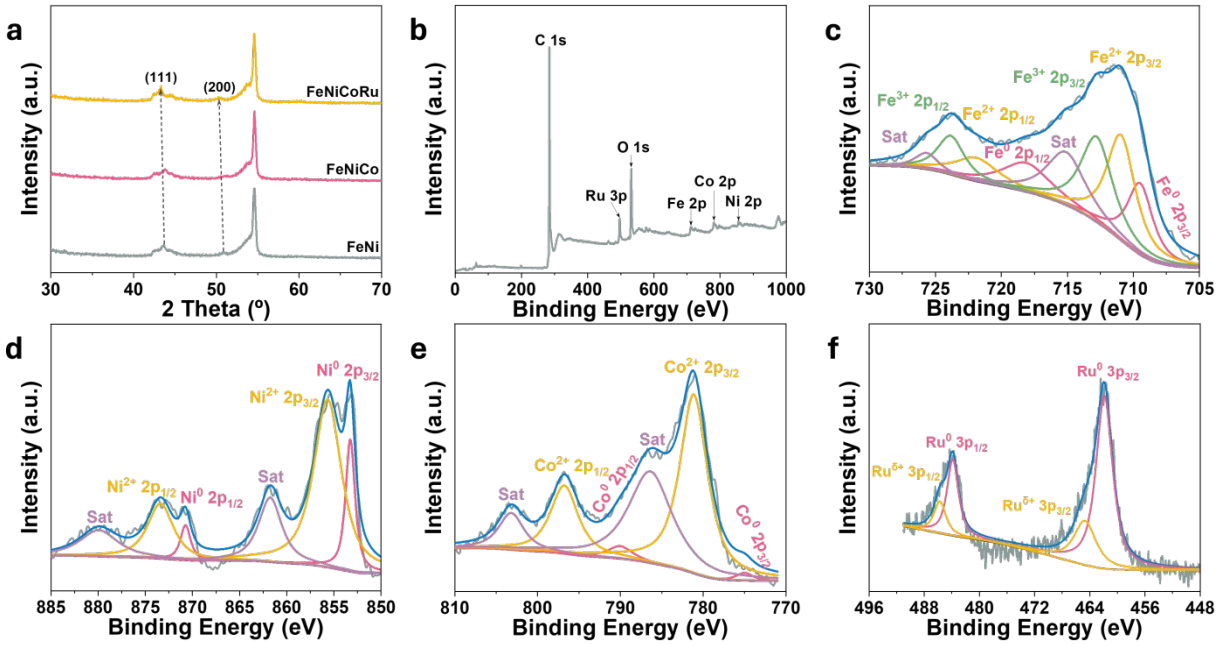

Figure 2. (**a**) XRD pattern of FeNiCoRu, FeNiCo, and FeNi NPs. (b) Full spectrum, high-resolution XPS spectra of (**b**) Fe 2p, (**c**) Co 2p, (**d**) Ni 2p, (**e**) Cr 2p, and (**f**) Ru 3p.

The electrocatalytic performance of the FeNiCoCrRu NPs for HER and OER were first evaluated using a typical three-electrode configuration in a neutral electrolyte (0.5 M NaCl), a simulated seawater electrolyte. All potentials were calibrated to the reversible hydrogen electrode (RHE) with 95% *i*R-correction. Cyclic voltammetry (CV) was conducted to electrochemically activate and stabilize the electrocatalysts followed by linear sweep voltammetry (LSV). As anticipated, the carbon paper alone exhibits negligible HER activity (**Figure 3a**), highlighting its inefficacy as a catalyst under the tested conditions. Pure Fe electrocatalyst demonstrates modest HER performance (**Figure 3a** and **Table S2**), requiring significant overpotentials of -0.640 V and -0.687 V to achieve current densities of -10 and -50 mA/cm², respectively. This high overpotential indicates limited efficiency, likely due to sluggish reaction kinetics and unfavorable adsorption characteristics on the Fe surface. HER activity improved incrementally as alloying elements were

introduced. The binary alloy FeNi and the ternary alloy FeNiCo both showed slightly better catalytic activity compared to pure Fe, indicating a synergistic effect due to the increased heterogeneity and potentially more favorable electronic structures brought by alloying.[31] However, the improvement was still moderate, suggesting that further compositional optimization was needed to achieve competitive performance. A significant leap in HER activity was observed upon the introduction of Ru into the FeNiCo alloy, forming the quaternary alloy FeNiCoRu NPs, which required overpotentials of only -0.368 V and -0.448 V to deliver current densities of 10 and 50 mA/cm², respectively. Remarkably, the HER activity of FeNiCoRu NPs approaches that of the benchmark Pt/C catalyst with overpotentials of -0.354 V and -0.457 V at 10 and 50 mA/cm², respectively, suggesting that the strategic incorporation of Ru creates active sites that are energetically favorable for the HER process. Our previous study indicated that Ni and Ru active sites stabilize different intermediates, with Ni facilitating H_2O adsorption and dissociation while Ru simultaneously accelerating combination of H* to H_2.[20, 35-36] This marked improvement can be attributed to Ru's well-known intrinsic HER activity, as well as its capability to modify the electronic environment of the alloy, enhancing hydrogen adsorption and desorption kinetics.[20, 31]

The Tafel slopes provide further insight into their reaction mechanisms (**Figure 3b** and **Table S2**).[37-38] The Fe, FeNi, and FeNiCo electrocatalysts exhibit relatively high Tafel slopes (181.8 mV/dec for Fe, 189.4 mV/dec for FeNi, and 158.3 mV/dec for FeNiCo), indicative of slow reaction kinetics and substantial energy barriers for HER. In contrast, the FeNiCoRu exhibits a notably lower Tafel slope (104.4 mV/dec), suggesting improved charge transfer and enhanced reaction kinetics. This reduction in Tafel slope underscores the beneficial impact of Ru, as it not only lowers the overpotential but also facilitates a more efficient catalytic pathway, closely resembling the behavior of Pt/C.[31] To quantify the exposed active sites on the electrocatalysts, electrochemical

surface area (ECSA) was determined from the double-layer capacitance in the non-Faradaic region (**Figure 3c** and **Figure S2**). Among these electrocatalysts, FeNiCoRu exhibits the highest ECSA value of 865.1 cm^2, significantly surpassing the values observed for FeNiCo (411.2 cm^2), FeNi (729.4 cm^2), and Fe (415.1 cm^2). A higher electrochemically active surface area (ECSA) reflects a higher density of active sites, which is directly associated with enhanced catalytic performance.

Furthermore, underpotential deposition of hydrogen (H_{UPD}) was conducted to explore hydrogen adsorption. H_{UPD} is a process where hydrogen atoms are adsorbed onto the surface of the electrocatalyst at potentials more positive than the equilibrium potential for hydrogen evolution, which provides valuable information about the surface structure and binding properties of the electrocatalyst.[39] As shown in **Figure S3**, no peaks corresponding to the oxidation and reduction of Ru-based oxides are observed.[39] The H_{UPD} peak of FeNiCoRu is stronger than those of Fe, FeNi and FeNiCo, implying a higher hydrogen adsorption capacity on FeNiCoRu.[40-41] Specifically, the favorable adsorption of H_2O leads to the formation of lots of hydrogen adsorbed on FeNiCoRu NPs, enhancing proton supply and subsequently promoting the hydrogen production process.

The OER activities of all electrocatalysts were evaluated under identical conditions to ensure comparability (**Figure 3d-3f**, and **Table S2**). The catalytic activity demonstrates a clear trend, following the order: FeNiCoRu > RuO_2 > FeNiCo > FeNi > Fe (**Figure 3d**). This sequence highlights that the incorporation of Ru into the catalyst structure significantly enhances the OER activity. Specifically, the introduction of Ru appears to favor a reaction pathway toward reduced energy barriers in the rate-determining step, thus improving overall reaction kinetics.[31] Specifically, FeNiCoRu requires overpotentials of 0.559 V and 0.710 V to deliver current densities of 10 and 80 mA/cm^2, respectively. Moreover, as illustrated in **Figures 3e**, the FeNiCoRu exhibits a notably small Tafel slope of 75.4 mV/decade, indicative of faster reaction kinetics and efficient charge

transfer. Furthermore, it possesses the largest ECSA (141.4 cm^2) (**Figure 3f** and **Figure S4**), suggesting a higher number of active sites available for electrocatalysis. This increased ECSA enhances the exposure of catalytic sites, contributing to the outstanding OER activity observed. Notably, the FeNiCoRu NPs are superior or comparable to the recently reported electrocatalysts for HER and OER (**Table S3**).

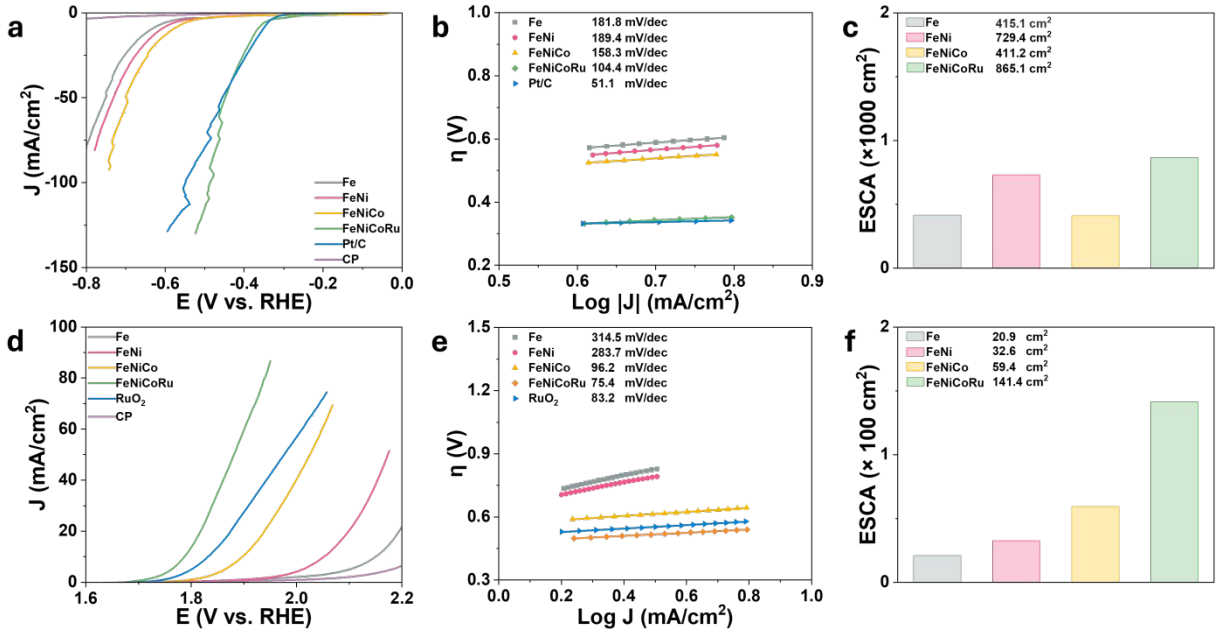

Figure 3. Neutral seawater electrolysis over Fe, FeNi, FeNiCo, FeNiCoRu, Pt/C, RuO_2 and carbon paper in 0.5 M NaCl electrolyte. LSV curves of (**a**) HER and (**d**) OER at a scan rate of 10 mV/s with 95% *i*R compensation. Tafel slope plots of (**b**) HER and (**e**) OER. ECSA and TOF plots of (**c**) HER and (**f**) OER.

Finally, the overall neutral seawater electrolysis was compared in two assembled full electrolyzers: FeNiCoRu||FeNiCoRu and Pt/C||RuO_2. As depicted in **Figure 4a**, the FeNiCoRu||FeNiCoRu electrolyzer requires the voltages of 2.272 V and 2.422 V to achieve current densities of 10 and 20 mA/cm^2, respectively, which is comparable to those of the Pt/C||RuO_2

electrolyzer (2.204 V and 2.347 V, respectively). To determine the Faradaic efficiency of the FeNiCoRu||FeNiCoRu electrolyzer, the hydrogen gas generated at the cathode was collected (**Figure 4b**), resulting in a calculated Faradaic efficiency of 98.2%. To evaluate the feasibility of the electrocatalysts for industrial applications, a long-term stability test was conducted on both FeNiCoRu||FeNiCoRu and Pt/C||RuO_2 electrolyzers using chronopotentiometry at a constant current density of 10 mA/cm^2 (**Figure 4e**). This stability is crucial for the development of economically viable electrolyzers for large-scale applications, as it directly impacts operational costs, energy efficiency, and the overall durability of the system. The results demonstrate that both electrolyzers exhibit comparable stability for neutral seawater electrolysis, with only a minimal increase in the applied voltage over time. Specifically, the FeNiCoRu||FeNiCoRu electrolyzer experiences a voltage rise of 0.161 V after 270 hours of continuous operation. Additionally, the comparable performance between the FeNiCoRu||FeNiCoRu and the Pt/C||RuO_2 electrolyzers underscores the potential of the FeNiCoRu NPs as a cost-effective alternative to precious metal-based catalysts, particularly in scenarios where scalability and cost-efficiency are key considerations. Such results are promising for the advancement of neutral seawater electrolysis technology, emphasizing the practical applicability of FeNiCoRu NPs. Future work would explore optimization strategies, including electrode architecture and electrolyte management, to enhance the stability and efficiency of these systems under industrial conditions.

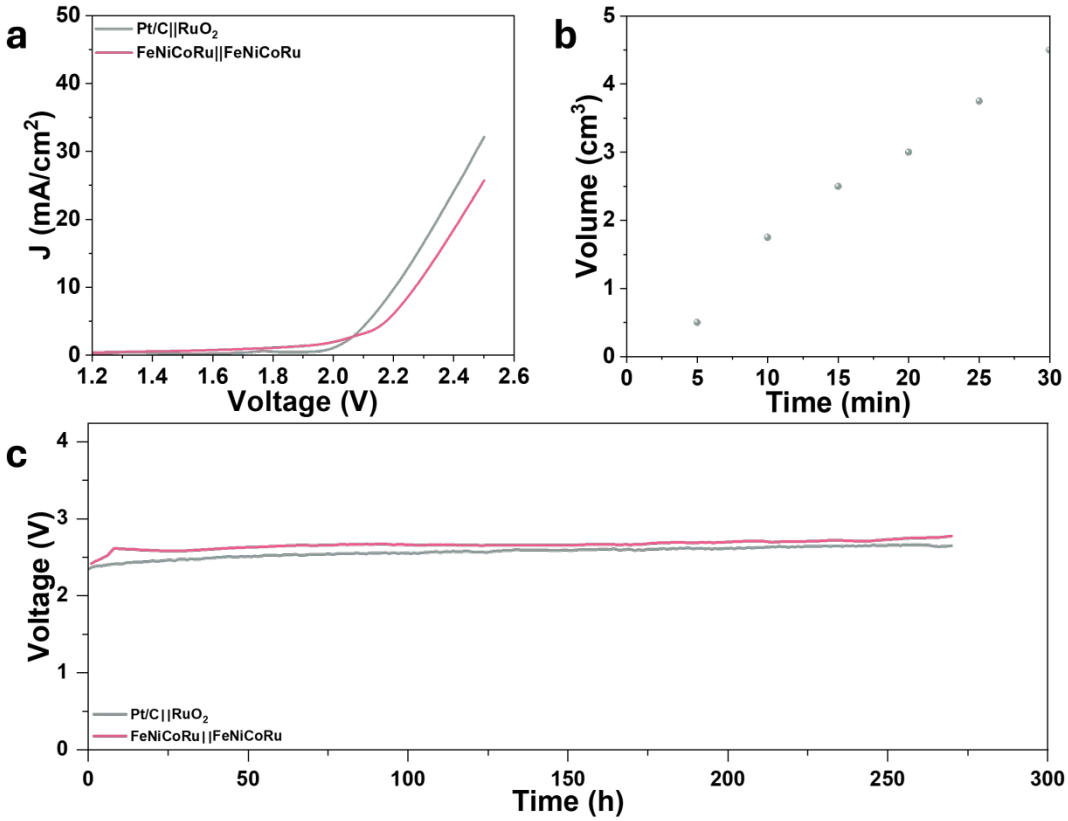

Figure 4. (**a**) LSV curves of FeNiCoRu||FeNiCoRu and Pt/C||RuO_2 electrolyzers in a simulated neutral seawater electrolyte (0.5 M NaCl). (**b**) The Faradaic efficiency for H_2 production. (**c**) Chronopotentiometry curves of FeNiCoRu||FeNiCoRu and Pt/C||RuO_2 electrolyzers at 10 mA/cm^2.

3. Conclusion

In summary, medium entropy alloy FeNiCoRu NPs were rapidly synthesized via a direct CO_2 laser induction technique under ambient conditions. The resulting material exhibits a porous, three-dimensional interconnected structure with microscale roughness, alongside a single-phase FCC crystal structure without evidence of phase separation or segregation. FeNiCoRu NPs showed superior electrocatalytic performance for both HER and OER during neutral seawater electrolysis, offering overpotentials of -0.368 V for HER and 0.559 V for OER at a current density of 10 mA/cm^2. When assembled into an electrolyzer, the FeNiCoRu||FeNiCoRu required voltages of

2.272 V and 2.422 V to deliver current densities of 10 mA/cm^2 and 20 mA/cm^2, respectively, demonstrating acceptable stability with a voltage increase of 0.161 V after 270 hours of continuous operation. The enhanced electrocatalytic activity of FeNiCoRu NPs primarily originates from the entropy-stabilizing effects, their porous and interconnected structure, and the multi-elemental composition, especially the incorporation of Ru. The synergistic effects lead to a reduction in reaction barriers and an improved catalytic efficiency. This work highlights the promise of FeNiCoRu NPs in bridging the gap between conventional electrocatalysts and practical, large-scale neutral seawater electrolysis, offering a pathway towards efficient green hydrogen generation. To advance these systems for industrial applications, future efforts will prioritize optimizing electrode structures and managing electrolyte composition to maximize both efficiency and stability.

4. Materials and Methods

4.1 Chemicals

Iron chloride ($FeCl_3 \cdot 6H_2O$, Sigma), nickel chloride ($NiCl_2 \cdot 6H_2O$, Fisher), cobalt chloride ($CoCl_2 \cdot 6H_2O$, Sigma), ruthenium chloride hydrate ($RuCl_3 \cdot xH_2O$, Aldrich), sodium citrate ($Na_3C_6H_5O_7 \cdot 2H_2O$, Sigma), Pt/C (20 wt%, Alfa Aesar), ruthenium oxide (RuO_2, Alfa Aesar), Nafion (D520, Fisher), ethanol (200 proof, Decon Labs), and sodium chloride (NaCl, Sigma) were all used as received without further purification. Carbon paper (AvCarb MGL370) was obtained from FuelCell.

4.2 Preparation of FeNiCoRu NPs

Carbon paper, measuring 1 cm × 1.2 cm, was thoroughly washed with deionized water and ethanol to remove any inorganic and organic residues. Next, a metal precursor solution containing

Fe, Ni, Co, Ru, and sodium citrate was drop-cast onto the carbon paper. After drying, the carbon paper was processed using a commercial CO_2 laser (Universal Laser Systems VLS3.50/60DT) and subsequently washed with deionized water. The laser power and scan rates were set to be 18 W and 10 cm/s, respectively. For comparison, three additional samples including FeNiCo, FeNi, and Fe samples were prepared under identical conditions, with only the compositions of the metal precursor solutions varying. Additional details can be found in Table S1.

4.3 Preparation of Pt/C and RuO_2

For comparison with conventional benchmarks, commercial Pt/C and RuO_2 electrocatalysts were also prepared. First, 4 mg of commercial electrocatalysts (Pt/C or RuO_2) was ultrasonicated in 1 mL of the mixture solution containing deionized water, ethanol and Nafion (*v*/*v*/*v* = 19/5/1) for 4 h. Then, 150 μL of the dispersion mixture was drop-cast onto CP and dried at 90 ºC on a hotplate. The loading mass of Pt/C and RuO_2 was calculated to be 0.5 mg/cm^2.

4.4 Material Characterization

PANalytical X'Pert Materials Research Diffractometer (λ = 0.15406 nm) was used to analyze the crystallinity of FeNiCoRu NPs. Helios 5 Hydra Dual Beam scanning electron microscope was employed to observe the surface morphology of FeNiCoRu NPs. FEI Tecnai F20 STEM was utilized to characterize the nanoparticle size and diffraction patterns. Kratos Axis 165 Photoelectron Spectrometer was used to analyze the surface chemical composition of FeNiCoRu NPs.

4.5 Electrochemical Measurements

Electrochemical measurements were conducted using a Biologic SP-200 electrochemical workstation in a three-electrode setup, with FeNiCoRu NPs acting as the working electrode, graphite as the counter electrode, and Ag/AgCl as the reference electrode. The electrolyte was a

0.5 M NaCl solution to replicate seawater conditions. All potentials were referred to the reversible hydrogen electrode (RHE), using the relationship $E_{RHE} = E(Ag/AgCl) + 0.635$ V. To activate the electrocatalysts, cyclic voltammetry (CV) was performed at a scan rate of 100 mV/s, while linear sweep voltammetry (LSV) was conducted at a scan rate of 10 mV/s. To analyze the impedance properties, electrochemical impedance spectroscopy (EIS) was employed at an overpotential of 0.3 V, with a frequency range from 0.1 Hz to 100 kHz and an AC amplitude of 5 mV. To estimate the double-layer capacitance (C_{dl}), CV measurements were carried out within non-Faradaic regions at various scan rates. The value of C_{dl} was determined by plotting the current density difference ($\Delta J = J_a - J_c$) at specific potentials against the scan rate. The electrochemical active surface area (ECSA) was then calculated using the equation ECSA = $C_{dl}/(C_s \times A)$, where C_s represents the specific capacitance of an atomically smooth planar surface (0.04 mF/cm^2) and A represents the geometric area of the electrode (1 cm^2). To assess the long-term stability, chronopotentiometry was measured at a constant current density of 10 mA/cm^2.

Acknowledgements

J. L. thanks the financial support from U.S. National Science Foundation (award numbers: 1825352 and 1933861), U.S. Department of Interior (grant number: R21AC10073-00), and U.S. Army Corps of Engineers, ERDC (grant number: W912HZ-21-2-0050).

Competing interests: all authors claim no competing interests.

Data and materials availability: All source data are available from the corresponding author upon reasonable request.

References

(1) J. Zhu, L. Hu, P. Zhao, L. Y. S. Lee, K.-Y. Wong. Recent Advances in Electrocatalytic Hydrogen Evolution Using Nanoparticles. *Chemical Reviews* 2020, 120, 851-918.
(2) L. Wan, Z. Xu, Q. Xu, M. Pang, D. Lin, J. Liu, B. Wang. Key components and design strategy of the membrane electrode assembly for alkaline water electrolysis. *Energy & Environmental Science* 2023, 16, 1384-1430.
(3) L. Quan, H. Jiang, G. Mei, Y. Sun, B. You. Bifunctional Electrocatalysts for Overall and Hybrid Water Splitting. *Chemical Reviews* 2024, 124, 3694-3812.
(4) H. Xie, Z. Zhao, T. Liu, Y. Wu, C. Lan, W. Jiang, L. Zhu, Y. Wang, D. Yang, Z. Shao. A membrane-based seawater electrolyser for hydrogen generation. *Nature* 2022, 612, 673-678.
(5) J. Guo, Y. Zheng, Z. Hu, C. Zheng, J. Mao, K. Du, M. Jaroniec, S.-Z. Qiao, T. Ling. Direct seawater electrolysis by adjusting the local reaction environment of a catalyst. *Nature Energy* 2023, 8, 264-272.
(6) H. Hu, Z. Zhang, L. Liu, X. Che, J. Wang, Y. Zhu, J. P. Attfield, M. Yang. Efficient and durable seawater electrolysis with a V_2O_3-protected catalyst. *Science Advances* 2024, 10, eadn7012.
(7) R. Fan, C. Liu, Z. Li, H. Huang, J. Feng, Z. Li, Z. Zou. Ultrastable electrocatalytic seawater splitting at ampere-level current density. *Nature Sustainability* 2024, 7, 158-167.
(8) T. Li, B. Wang, Y. Cao, Z. Liu, S. Wang, Q. Zhang, J. Sun, G. Zhou. Energy-saving hydrogen production by seawater electrolysis coupling tip-enhanced electric field promoted electrocatalytic sulfion oxidation. *Nature Communications* 2024, 15, 6173.
(9) T. Liu, Z. Zhao, W. Tang, Y. Chen, C. Lan, L. Zhu, W. Jiang, Y. Wu, Y. Wang, Z. Yang, D. Yang, Q. Wang, L. Luo, T. Liu, H. Xie. In-situ direct seawater electrolysis using floating platform in ocean with uncontrollable wave motion. *Nature Communications* 2024, 15, 5305.
(10) H. Jin, J. Xu, H. Liu, H. Shen, H. Yu, M. Jaroniec, Y. Zheng, S.-Z. Qiao. Emerging materials and technologies for electrocatalytic seawater splitting. *Science Advances* 2023, 9, eadi7755.
(11) F. Shiokawa, A. Asilah Haji Tajuddin, T. Ohto, Y. Yu, T. Fujita, H. Tanimoto, Z. Xi, S. Jeong, Y. Ito. Durable high-entropy non-noble metal anodes for neutral seawater electrolysis. *Chemical Engineering Journal* 2024, 479, 147862.
(12) L. P. Phan, T. T. N. Tran, T.-K. Truong, J. Yu, H.-V. T. Nguyen, T. B. Phan, N. H. Thi Tran, N. Q. Tran. Highly Efficient and Stable Hydrogen Evolution from Natural Seawater by Boron-Doped Three-Dimensional Ni_2P–MoO_2 Heterostructure Microrod Arrays. *The Journal of Physical Chemistry Letters* 2023, 14, 7264-7273.
(13) T. T. N. Tran, T.-K. Truong, J. Yu, L. Peng, X. Liu, L. H. T. Nguyen, S. Park, Y. Kawazoe, T. B. Phan, N. H. T. Tran, N. H. Vu, N. Q. Tran. Dopant-Induced Charge Redistribution on the 3D Sponge-like Hierarchical Structure of Quaternary Metal Phosphides Nanosheet Arrays Derived from Metal–Organic Frameworks for Natural Seawater Splitting. *ACS Applied Materials & Interfaces* 2024, 16, 2270-2282.
(14) X. Zou, Y. Zhang. Noble metal-free hydrogen evolution catalysts for water splitting. *Chemical Society Reviews* 2015, 44, 5148-5180.
(15) Y. Li, Y. Sun, Y. Qin, W. Zhang, L. Wang, M. Luo, H. Yang, S. Guo. Recent Advances on Water-Splitting Electrocatalysis Mediated by Noble-Metal-Based Nanostructured Materials. *Advanced Energy Materials* 2020, 10, 1903120.
(16) Y. Shi, B. Zhang. Recent advances in transition metal phosphide nanomaterials: synthesis and applications in hydrogen evolution reaction. *Chemical Society Reviews* 2016, 45, 1529-1541.
(17) E. P. George, D. Raabe, R. O. Ritchie. High-entropy alloys. *Nature Reviews Materials* 2019, 4, 515-534.

(18) Y. Sun, S. Dai. High-entropy materials for catalysis: A new frontier. *Science Advances* 2021, 7, eabg1600.
(19) Y. Yao, Q. Dong, A. Brozena, J. Luo, J. Miao, M. Chi, C. Wang, I. G. Kevrekidis, Z. J. Ren, J. Greeley, G. Wang, A. Anapolsky, L. Hu. High-entropy nanoparticles: Synthesis-structure-property relationships and data-driven discovery. *Science* 2022, 376, eabn3103.
(20) Y. Xie, S. Xu, A. C. Meng, B. Zheng, Z. Chen, J. M. Tour, J. Lin. Laser-induced high-entropy alloys as long-duration bifunctional electrocatalysts for seawater splitting. *Energy & Environmental Science* 2024, 17, 8670-8682.
(21) Y. Ma, Y. Ma, Q. Wang, S. Schweidler, M. Botros, T. Fu, H. Hahn, T. Brezesinski, B. Breitung. High-entropy energy materials: challenges and new opportunities. *Energy & Environmental Science* 2021, 14, 2883-2905.
(22) X. Wang, Q. Peng, X. Zhang, X. Lv, X. Wang, Y. Fu. Carbonaceous-assisted confinement synthesis of refractory high-entropy alloy nanocomposites and their application for seawater electrolysis. *Journal of Colloid and Interface Science* 2022, 607, 1580-1588.
(23) N. Kang, H. Ma, M. Chu, X. Jiang, Z. Liu, X. Feng, X. Ren, X. Liu, G. Xie. Electrochemical performance of in-situ electrodeposited spinel-structured high entropy oxides/NiFeCuMoMn-high entropy alloy multiphase electrocatalysts for seawater electrolysis. *Electrochimica Acta* 2024, 506, 144931.
(24) Y. Yao, Z. Huang, P. Xie, S. D. Lacey, R. J. Jacob, H. Xie, F. Chen, A. Nie, T. Pu, M. Rehwoldt, D. Yu, M. R. Zachariah, C. Wang, R. Shahbazian-Yassar, J. Li, L. Hu. Carbothermal shock synthesis of high-entropy-alloy nanoparticles. *Science* 2018, 359, 1489-1494.
(25) L. Cheng, C. S. Yeung, L. Huang, G. Ye, J. Yan, W. Li, C. Yiu, F.-R. Chen, H. Shen, B. Z. Tang, Y. Ren, X. Yu, R. Ye. Flash healing of laser-induced graphene. *Nature Communications* 2024, 15, 2925.
(26) W. Guo, S. Zhang, J. Zhang, H. Wu, Y. Ma, Y. Song, L. Cheng, L. Chang, G. Li, Y. Liu, G. Wei, L. Gan, M. Zhu, S. Xi, X. Wang, B. I. Yakobson, B. Z. Tang, R. Ye. Accelerating multielectron reduction at CuxO nanograins interfaces with controlled local electric field. *Nature Communications* 2023, 14, 7383.
(27) M. Fang, G. Dong, R. Wei, J. C. Ho. Hierarchical Nanostructures: Design for Sustainable Water Splitting. *Advanced Energy Materials* 2017, 7, 1700559.
(28) L. Wu, F. Zhang, S. Song, M. Ning, Q. Zhu, J. Zhou, G. Gao, Z. Chen, Q. Zhou, X. Xing, T. Tong, Y. Yao, J. Bao, L. Yu, S. Chen, Z. Ren. Efficient Alkaline Water/Seawater Hydrogen Evolution by a Nanorod-Nanoparticle-Structured Ni-MoN Catalyst with Fast Water-Dissociation Kinetics. *Advanced Materials* 2022, 34, 2201774.
(29) C. Liang, P. Zou, A. Nairan, Y. Zhang, J. Liu, K. Liu, S. Hu, F. Kang, H. J. Fan, C. Yang. Exceptional performance of hierarchical Ni–Fe oxyhydroxide@NiFe alloy nanowire array electrocatalysts for large current density water splitting. *Energy & Environmental Science* 2020, 13, 86-95.
(30) Z. Yu, D. W. Boukhvalov, H. Tan, D. Xiong, C. Feng, J. Wang, W. Wang, Y. Zhao, K. Xu, W. Su, X. Xiang, F. Lin, H. Huang, F. Zhang, L. Zhang, L. Meng, L. Liu. Sulfur and phosphorus co-doped FeCoNiCrMn high-entropy alloys as efficient sulfion oxidation reaction catalysts enabling self-powered asymmetric seawater electrolysis. *Chemical Engineering Journal* 2024, 494, 153094.
(31) J. Hao, Z. Zhuang, K. Cao, G. Gao, C. Wang, F. Lai, S. Lu, P. Ma, W. Dong, T. Liu, M. Du, H. Zhu. Unraveling the electronegativity-dominated intermediate adsorption on high-entropy alloy electrocatalysts. *Nature Communications* 2022, 13, 2662.

(32) Q. Wang, Z. Jia, J. Li, Y. He, Y. Yang, Y. Li, L. Sun, B. Shen. Attractive Electron Delocalization Behavior of FeCoMoPB Amorphous Nanoplates for Highly Efficient Alkaline Water Oxidation. *Small* 2022, 18, 2204135.
(33) Z. Zhang, J. Cai, H. Zhu, Z. Zhuang, F. Xu, J. Hao, S. Lu, H. Li, F. Duan, M. Du. Simple construction of ruthenium single atoms on electrospun nanofibers for superior alkaline hydrogen evolution: A dynamic transformation from clusters to single atoms. *Chemical Engineering Journal* 2020, 392, 123655.
(34) Z. Qingqing, R. Li, Z. Li, Y. Yongqiang, L. Xiaohao. Mild and scalable synthesis of a high performance $CrFeCoNiRu_{0.05}$ high entropy nano-alloy/carbon electrocatalyst for efficient urea production with a chelate-based ionic liquid. *New Journal of Chemistry* 2024, 48, 9738-9747.
(35) Y. Zeng, M. Zhao, Z. Huang, W. Zhu, J. Zheng, Q. Jiang, Z. Wang, H. Liang. Surface Reconstruction of Water Splitting Electrocatalysts. *Advanced Energy Materials* 2022, 12, 2201713.
(36) H. Liang, A. N. Gandi, D. H. Anjum, X. Wang, U. Schwingenschlögl, H. N. Alshareef. Plasma-Assisted Synthesis of NiCoP for Efficient Overall Water Splitting. *Nano Letters* 2016, 16, 7718-7725.
(37) H. Deng, C. Zhang, Y. Xie, T. Tumlin, L. Giri, S. P. Karna, J. Lin. Laser induced MoS_2/carbon hybrids for hydrogen evolution reaction catalysts. *Journal of Materials Chemistry A* 2016, 4, 6824-6830.
(38) Y. Xie, C. Zhang, X. He, T. White, J. D. Demaree, M. Griep, J. Lin. Monolithic electrochemical cells for overall water splitting. *Journal of Power Sources* 2018, 397, 37-43.
(39) A. Kundu, S. K. Dey, S. Dey, A. Anoop, S. Mandal. Mononuclear Ruthenium-Based Water Oxidation Catalyst Supported by Anionic, Redox-Non-Innocent Ligand: Heterometallic O–O Bond Formation via Radical Coupling Pathway. *Inorganic Chemistry* 2020, 59, 1461-1470.
(40) Q. He, Y. Zhou, H. Shou, X. Wang, P. Zhang, W. Xu, S. Qiao, C. Wu, H. Liu, D. Liu, S. Chen, R. Long, Z. Qi, X. Wu, L. Song. Synergic Reaction Kinetics over Adjacent Ruthenium Sites for Superb Hydrogen Generation in Alkaline Media. *Advanced Materials* 2022, 34, 2110604.
(41) H. Chen, X. Ai, W. Liu, Z. Xie, W. Feng, W. Chen, X. Zou. Promoting Subordinate, Efficient Ruthenium Sites with Interstitial Silicon for Pt-Like Electrocatalytic Activity. *Angewandte Chemie International Edition* 2019, 58, 11409-11413.

Data Availability Statement

The data supporting this article have been included as part of the Supplementary Information.